Improved PML for the FDTD Solution of Wave-Structure Interaction Problems

Jean-Pierre Bérenger

Invited Paper

***Abstract*— In a previous paper, an optimum perfectly matched layer has been designed for the finite-difference time-domain (FDTD) solution of wave-structure interaction problems. The present paper shows the results of subsequent investigations that were done with the intention of reducing the thickness of this optimum PML. Four improvements to the PML are presented. The resulting reductions of the thickness are discussed.**

***Index Terms*—FTTD methods.**

I. Introduction

The perfectly matched layer [1], [2] is an absorbing boundary condition developed to simulate free space with the finite-difference time-domain (FDTD) technique [3]. In [4], the numerical reflection that arises when solving wave-structure interaction problems is analyzed, and the specifications of an optimum PML are determined with the intention of reducing as much as possible the computational requirements. By using this PML the scatterer-PML separation can be very small, resulting in computational domains widely shorter than those required by methods of free-space simulation, such as [5] or [6]. Nevertheless, the optimum PML [4] is not ideal since in most applications its thickness must be at least on the order of ten cells, so that its computational cost is not negligible as compared to that of the inner domain [7]. For this reason, efforts have been done with the intention of reducing the thickness of this PML. We present the results of such investigations.

Four methods that allow the PML thickness to be reduced are discussed. The first one is based on the splitting of the subcomponents of the electromagnetic field into two parts, the second one on the use of an absorbing matched medium in the inner domain, the third one on the replacement of the perfect electric condition by an operator [6] on the outer boundary of the PML, and the last one consists in expanding the mesh in the PML. None of these methods yields an ideal PML, allowing the computational time to be negligible, say, a two- or three-cell thick PML. Nevertheless, real reductions of computational time can be achieved. As [4], the present paper is mainly devoted to the two-dimensional (2-D) case, although the three-dimensional (3-D) case is considered in some comments and discussions.

Manuscript received March 13, 1996; revised October 7, 1996.

The author is with the Centre d'Analyze de Défense 16 bis, Arcueil, 94114, France.

Publisher Item Identifier S 0018-926X(97)02295-3.

II. The Basic PML

When solving wave-structure interaction problems, the PML must satisfy three conditions [4]. The normal reflection coefficient $R(0)$ must be of the order of 1%, the growth of the conductivity from one cell to the next must be smaller than a certain value, and the numerical conductivity $\sigma_n(0)$ in the vacuum-layer interface must satisfy

$$\sigma_n(0) \leq \frac{1}{\Theta}\frac{2\pi\varepsilon_0}{D_c} \tag{1}$$

where D_c is the duration of the computation and Θ is a margin factor set on the order of ten. From such conditions, the optimum profile of conductivity is the following geometric progression of ratio g:

$$\sigma(\rho) = \sigma_0 g^{\frac{\rho}{\Delta x}} = -\frac{\varepsilon_0 c}{2\Delta x}\frac{\ln g}{g^N - 1}\ln R(0) g^{\frac{\rho}{\Delta x}} \tag{2}$$

where N is the number of cells in the PML thickness, ρ the distance from the interface, and Δx the size of the FDTD cell. Then, the PML thickness must be at least equal to

$$N = \frac{1}{\ln g}\ln\left[1 - \frac{c}{4\pi}(\sqrt{g} - 1)\ln R(0)\frac{\Theta}{\Delta x}D_c\right]. \tag{3}$$

As Θ, the ratio g is an empirical data and has been found as a function of the number of cells in the scatterer length. An empirical formula is given in [4].

In [4], the condition (1) is interpreted by considering that the first row of the PML produces some reflection as if this row were the first one of a conductive medium of conductivity $\sigma_n(0)$. Frequencies lower than

$$f_c = \frac{1}{t_c} = \frac{\sigma_n(0)}{2\pi\varepsilon_0} \tag{4}$$

are reflected, while higher frequencies are not reflected.

III. The Split PML and the PML-A Version

As discussed in [4], the numerical reflection from a PML originates in the shift between electric and magnetic conductivities in the FDTD implementation. With the intention of reducing this reflection, we have designed a new PML medium in which each subcomponent of the field is split into two parts in such a way that different conductivities can be assigned to each part. Two possible uses of this medium are presented below—the first one is in use in 3-D computer codes known as the PML-A version of the PML method [8].

A. The Split PML Medium

In the 2-D TE case [1, 4], there are four subcomponents in the PML medium—E_x, E_y, H_{zx}, H_{zy}—connected through four equations. Here, we split these subcomponents into eight quantities that we denote by E_{xa}, E_{xb}, E_{ya}, E_{yb}, H_{zxa}, H_{zxb}, H_{zya}, H_{zyb}, and we replace the four equations in [1] by the following:

$$\varepsilon_0 \frac{\partial E_{xa}}{\partial t} + \sigma_{ya} E_{xa} = p_a \frac{\partial (H_{zxa} + H_{zxb} + H_{zya} + H_{zyb})}{\partial y} \tag{5a}$$

$$\varepsilon_0 \frac{\partial E_{xb}}{\partial t} + \sigma_{yb} E_{xb} = p_b \frac{\partial (H_{zxa} + H_{zxb} + H_{zya} + H_{zyb})}{\partial y} \tag{5b}$$

$$\varepsilon_0 \frac{\partial E_{ya}}{\partial t} + \sigma_{xa} E_{ya} = -p_a \frac{\partial (H_{zxa} + H_{zxb} + H_{zya} + H_{zyb})}{\partial x} \tag{5c}$$

$$\varepsilon_0 \frac{\partial E_{yb}}{\partial t} + \sigma_{xb} E_{yb} = -p_b \frac{\partial (H_{zxa} + H_{zxb} + H_{zya} + H_{zyb})}{\partial x} \tag{5d}$$

$$\mu_0 \frac{\partial H_{zxa}}{\partial t} + \sigma^*_{xa} H_{zxa} = -p_a \frac{\partial (E_{ya} + E_{yb})}{\partial x} \tag{5e}$$

$$\mu_0 \frac{\partial H_{zxb}}{\partial t} + \sigma^*_{xb} H_{zxb} = -p_b \frac{\partial (E_{ya} + E_{yb})}{\partial x} \tag{5f}$$

$$\mu_0 \frac{\partial H_{zya}}{\partial t} + \sigma^*_{ya} H_{zya} = p_a \frac{\partial (E_{xa} + E_{xb})}{\partial y} \tag{5g}$$

$$\mu_0 \frac{\partial H_{zyb}}{\partial t} + \sigma^*_{yb} H_{zyb} = p_b \frac{\partial (E_{xa} + E_{xb})}{\partial y} \tag{5h}$$

with

$$p_a + p_b = 1. \tag{5i}$$

We note that this medium reduces to that of [1] if the conductivities of index a and b are equal or if either p_a or p_b equals zero. A similar theory as that in [1] shows that the features of this eight-subcomponent medium are identical to those of the four-subcomponent medium. Most quantities defined in [1] are valid with (5), except w_x and w_y, which must be replaced by

$$w_u = \frac{\frac{p_a}{1 - i\sigma^*_{ua}/\mu_0\omega} + \frac{p_b}{1 - i\sigma^*_{ub}/\mu_0\omega}}{\frac{p_a}{1 - i\sigma_{ua}/\varepsilon_0\omega} + \frac{p_b}{1 - i\sigma_{ub}/\varepsilon_0\omega}} \quad (u = x, y). \tag{6}$$

The reflection from an interface located between a vacuum and a medium whose transverse conductivities equal zero is given by the same formula as that in [1]. At an interface normal to x, if $\sigma_{ya} = \sigma_{yb} = \sigma^*_{ya} = \sigma^*_{yb} = 0$, we have

$$r = \frac{1 - \sqrt{w_x}}{1 + \sqrt{w_x}}. \tag{7}$$

From (6) and (7), there is no reflection from this interface if the two couples of conductivities (σ_{xa}, σ^*_{xa}) and (σ_{xb}, σ^*_{xb}) satisfy the usual matching impedance condition. As a result, an absorbing reflectionless layer can be built on the outer boundary of a FDTD domain, using (5) in place of the initial PML medium [1]. The medium (5) can be generalized to three dimensions. Then there are 24 subcomponents in the medium in which (6) and (7) are also valid.

B. The PML-A Version

The PML-A version of the PML technique consists of using (5) only in the vacuum-layer interface and the initial medium [1] elsewhere. From a theoretical point of view, one can also consider that (5) is used everywhere, with conductivities of index a and b equal except in the interface. In practice, using (5) only in the interface adds a very small computational cost (see below). Let us now consider a layer normal to x. In the interface, the component E_y is split into E_{ya} and E_{yb} computed by (5c) and (5d). These equations involve two conductivities, σ_{xa} and σ_{xb}. Their numerical values used in the discretized equations, denoted by $\sigma_{an}(0)$ and $\sigma_{bn}(0)$, are set as follows:

$$\sigma_{an}(0) = \sigma_n(0) \qquad \sigma_{bn}(0) = 0 \tag{8}$$

where $\sigma_n(0)$ is the numerical conductivity in the interface of the basic PML [4]. Since the magnetic conductivities are not present in the interface, let us enforce $\sigma^*_{xa} = \sigma^*_{xb} = 0$ into (6). With $\sigma_{xa} = \sigma_{an}(0) = \sigma_n(0)$ and $\sigma_{xb} = \sigma_{bn}(0) = 0$, at frequencies lower than the cutoff (4), this is $\varepsilon_o\, \omega << \sigma_n(0)$, we have

$$w_x = \frac{p_a + p_b}{0 + p_b} = \frac{1}{p_b} \tag{9}$$

so that the reflection coefficient (7) becomes

$$r = \frac{\sqrt{p_b} - 1}{\sqrt{p_b} + 1}. \tag{10}$$

To reduce the numerical reflection, we set (10) equal to $\frac{1}{2}$ expecting that half of this reflection would be produced by the interface and the other half by the second row of the mesh. Since the conductivities of these rows are electric and magnetic ones, respectively, the two contributions will have opposite signs. We may expect them to cancel one another. Setting $r = -1/2$ in (10) yields the parameter p_b to be used to achieve such a process. We obtain

$$p_a = \frac{8}{9} \qquad p_b = \frac{1}{9}. \tag{11}$$

Some results are shown in Fig. 1 for 20-cell and 100-cell plates. The computational conditions are those in [4], with a scatterer-PML separation of two cells (as in all the experiments reported in the present paper). The field in Fig. 1 is the normal electric component at the end of the plates (test point 2 in Fig. 2). As expected, using the PML-A version in place of the basic PML allows the numerical reflection to be widely reduced after the cutoff time t_c. But this reflection is not canceled so that PML-A does not allow condition (1) not to be satisfied. Actually, in practice PML-A is used to reduce the margin Θ in (1). In Fig. 1, one can observe that the PML-A results later depart from the reference. Fig. 2 shows detailed results for six test points on the 100-cell plate. At points 1, 2, and 3 close to the end of the plate, where the largest values of the field are observed, PML-A results are better than PML

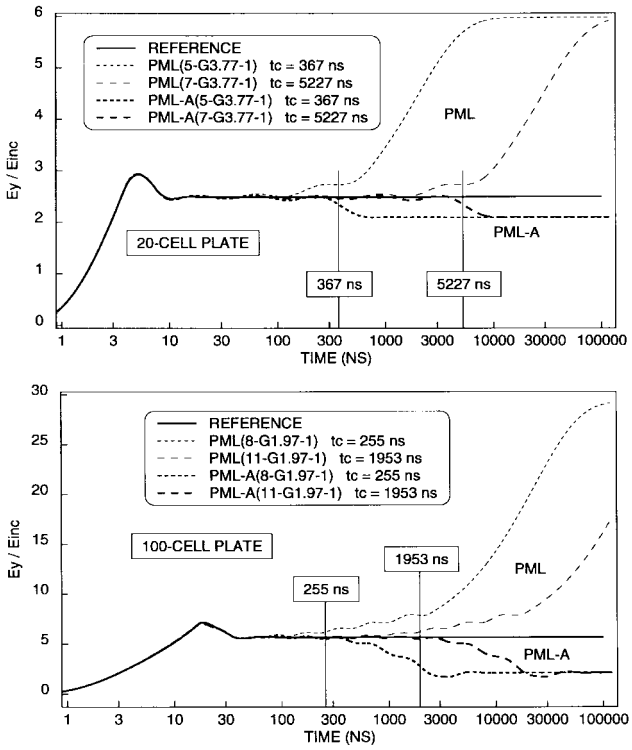

Fig. 1. Comparison of the PML-A version with the basic PML. Electric field at the end of 20-cell and 100-cell plates.

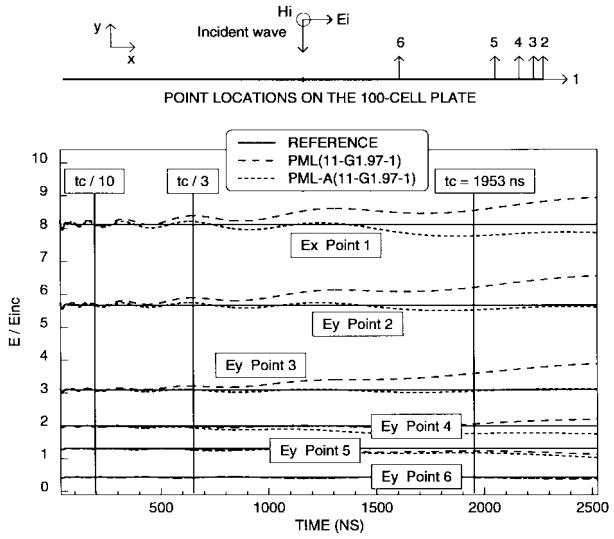

Fig. 2. Comparison of the PML-A version with the basic PML around time t_c.

ones. Conversely, at points 4 and 5, where the field is small, PML-A is worse than PML. Nevertheless, before time $t_c/3$ all the PML-A results are close to the reference, so that Fig. 2 suggests that Θ could be set on the order of three instead of ten with the basic PML. We also observed that $\Theta = 3$ is sufficient to insure correct results with other 2-D and 3-D scatterers [9], instead of Θ in the range five to ten with the basic PML. From (3), the resulting reduction of the PML thickness N can be estimated by considering that N approximately varies as $ln\ (\Theta)\ /lng$. For reductions of Θ in the range 2–3 and g in the range 3–1.5, the thickness is decreased by 0.6–3 cells.

Starting from a basic version of the PML method, the implementation of the PML-A version only requires small sets of instructions to be added to the code. In the 3-D case, for example at an interface normal to x, E_{yx} and E_{zx}must be replaced by E_{yxa}, E_{yxb}, E_{zxa}, E_{zxb} computed by discretizing the 3-D counterparts of (5c) and (5d). An easy and efficient implementation consists in storing E_{yxa}, E_{yxb}, E_{zxa}, E_{zxb}, in extra arrays, and the sums $E_{yxa} + E_{yxb}$, $E_{zxa} + E_{zxb}$ in the normal E_{yx}, E_{zx} arrays, so that the basic code can be left unchanged at magnetic points located on both sides of the interface, the sums of a and b parts being automatically taken into account in the spatial derivatives.

The extra computational time from the PML-A interface can be estimated by considering that there are 12 unknowns to be computed in the first cell of the side layers, in place of ten. Another estimation could be based on the number of operations. The PML-A interface adds ten operations per cell, to be compared to the 56 operations in a normal PML cell. Both evaluations yield extra requirements that are small parts (2/10 and 10/56) of the requirements of a normal PML cell. Numerical experiments confirmed such estimates. On a workstation the cost of PML-A was measured in the range 1/5–1/3 the cost of adding one cell to the PML thickness. As a result, the computational time is reduced by using the PML-A version since such a cost is small as compared with the reduction of thickness mentioned above (0.6–3 cells). The resulting overall savings are typically in the range 5–15% with 3-D 100-cell scatterers. Such a gain is small, but it can be obtained by a very small effort of encoding, as emphasized above. In our 3-D code [8], we implemented the PML-A version as standard PML.

C. The Split PML

Fig. 3 shows some results computed using the medium (5) everywhere in the absorbing layer. The numerical conductivities were the following, at mesh index L:

$$\sigma_{an}(L) = \sigma_n(L)$$

$$\sigma_{bn}(L) = \frac{\sigma_n(L)}{s} \tag{12}$$

where s is a parameter larger than one and $\sigma_n(L)$ the numerical conductivity of the basic PML [4]. To ensure a sufficient absorption of the b subcomponents, it can be shown that $ln(s)/ln(g)$ cells must be added to the PML thickness. The results in Fig. 3 were computed with $g = 10$, $s = 10$, 100, 1000, and $p_a = 0.95$. It was found that this value of p_a yields the best results in this experiment. With $s = 1000$, the magnitude of the oscillations is about 1%, on the order of that obtained with the basic PML and $g = 2$. Thus, PML-D allows larger g to be used, so that a substantial reduction of the thickness of the PML can be expected. But some disadvantages are the empirical parameter p_a, the extra computational cost per cell since there are 14 unknowns per 3-D cell in side layers, and the two or three extra cells required to ensure a sufficient absorption, so that PML-D could only be interesting when dealing with long time calculations requiring very thick PML's. Actually, up to

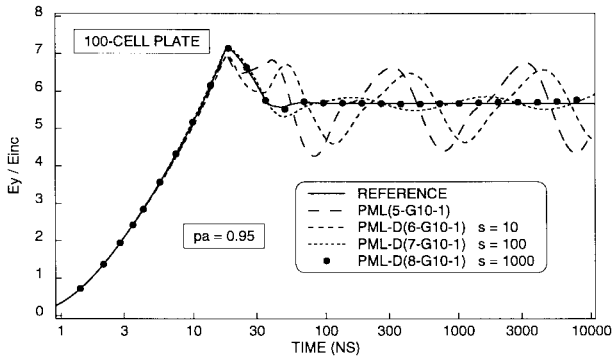

Fig. 3. Electric field computed using a split PML (PML-D) in the whole layer, for three values of the parameter s.

now we have not investigated PML-D in the 3-D case. The reason is that another version described in the next section allows the thickness of the PML to be reduced in long time calculations, and encoding this version is much easier than PML-D.

IV. Matched Medium and the PML-B Version

With the improvement described in this section, the numerical reflection produced by the first row of the PML is removed, so that condition (1) is no longer required. To obtain such an achievement, the basic idea is the replacement of the vacuum around the scatterer by a classical matched medium whose impedance equals that of vacuum and whose conductivity σ_v is set on the order of the numerical conductivity of the interface $\sigma_n(0)$. This modification of the PML method must satisfy two conditions. First, the physical reflection from the matched medium-PML interface must be equal to zero. Second, the absorption of the scattered field must be negligible in the matched medium. Both conditions are addressed below.

The absence of reflection from the MM-PML interface is ensured by the implementation shown in Fig. 4. In the PML, the longitudinal conductivities grow geometrically as in the basic PML, and the transverse conductivities are equal to the MM conductivities σ_v and $\sigma_v^* = \sigma_v \mu_0/\varepsilon_0$. Since the matched medium can be viewed as a PML(σ_v, σ_v^*, σ_v, σ_v^*), the interface is located between two PML media having the same transverse conductivities. So, from [1], [2] there is no physical reflection from this interface. Let us now consider the second condition. In the MM, a plane wave is absorbed according to

$$\psi(r) = \psi(0) e^{-\frac{\sigma_v}{\varepsilon_0 c} r}. \tag{13}$$

Denoting by L_s the length of the scatterer, the transmission on this length is

$$B = e^{-\frac{\sigma_v}{\varepsilon_0 c} L_s}. \tag{14}$$

It has been empirically found (see below) that the absorption of the scattered field is negligible in the MM if B is chosen at least equal to 0.99. This is an absorption of 1% on the scatterer length. As a result, the MM conductivity σ_v must satisfy the condition

$$\sigma_v \leq -\frac{\varepsilon_0 c}{L_S} \ln B \quad (B \approx 0.99). \tag{15}$$

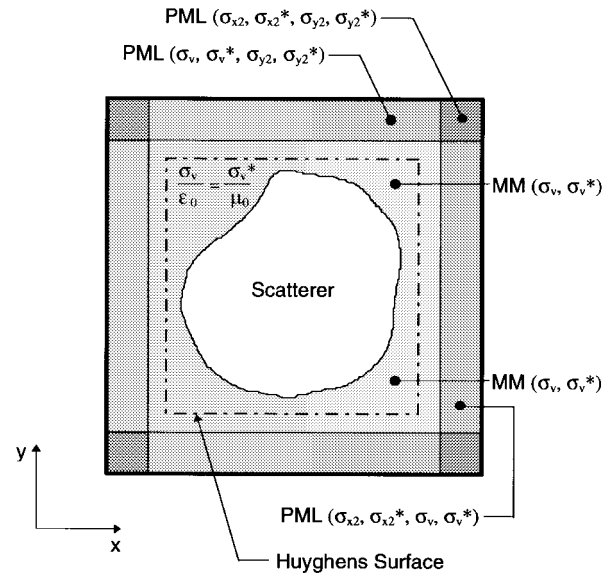

Fig. 4. The PML-B computational domain. Inner domain filled with a matched medium (MM).

To remove the numerical reflection from the MM-PML interface, σ_v must be on the order of the conductivity of the interface. For consistency with the ratios of conductivities in the PML, we chose σ_v as

$$\sigma_v = \frac{\sigma_0}{\sqrt{g}} = \frac{1}{\sqrt{g}} \frac{\varepsilon_0 c}{2\Delta x} \frac{\ln g}{1 - g^N} \ln R(0). \tag{16}$$

The numerical conductivity of the interface (average value in the cell) is then slightly different from that of the basic PML [4]

$$\begin{aligned} \sigma_n(0) &= \sigma_0 \left(\frac{1}{2\sqrt{g}} + \frac{\sqrt{g} - 1}{\ln g} \right) \\ &= \frac{\varepsilon_0 c \left(\sqrt{g} - 1 + \frac{\ln g}{2\sqrt{g}} \right)}{2\Delta x (1 - g^N)} \ln R(0). \end{aligned} \tag{17}$$

Some experiments are shown in Fig. 5, with 20-cell and 100-cell plates. Electric and magnetic fields are plotted. With each plate, the computations were performed using PML-B's of same ratios g but various thickness N and then various σ_0 and σ_v from (16). For each PML-B, transmission B from (14) and cutoff t_c from (4) are reported in the figure. According to (16), as the number of cells N increases, the conductivities σ_0 and σ_v decrease, so that B approaches one. With $B < 0.9$, both fields are not exact. The absorption in the MM is too strong. With $B = 0.99$, the results are very close to the reference. Similar results were observed with other 2-D and 3-D scatterers. We can also note in Fig. 5 that the electric field does not depart from the reference after time t_c. As expected, there is no numerical reflection from the MM-PML interface.

For a given g, the number of cells in the PML that allows the MM absorption to be negligible can be found from (15) and (16)

$$N_B = \frac{1}{\ln g} \left[1 + \frac{\ln g}{2\sqrt{g}} \frac{\ln R(0)}{\ln B} \frac{L_S}{\Delta x} \right]. \tag{18}$$

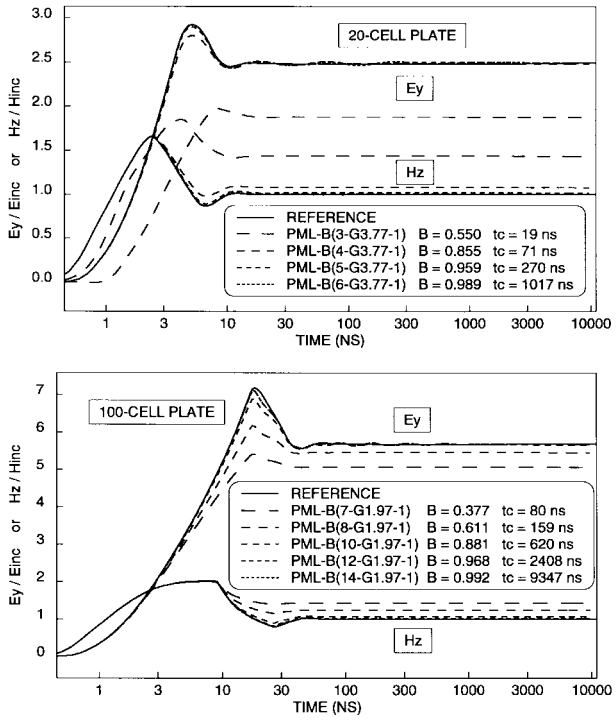

Fig. 5. Electric and magnetic fields on 20-cell and 100-cell plates computed using various PML-B layers.

With $R(0) = 0.01$, $B = 0.99$, and a N_S-cell scatterer ($N_S \Delta x = L_S$), we have

$$N_B = \frac{1}{\ln g} \ln \left[1 + 229 \frac{\ln g}{\sqrt{g}} N_S \right]. \tag{19}$$

For 20-cell and 100-cell scatterers, with $g = 3.77$ and 1.97, respectively, (19) gives $N_B = 6.06$ and 13.73. Since the thickness N_B does not depend on the duration of the computation D_c, the PML-B may be either thinner or thicker than the basic PML or the PML-A, depending on D_c. Equating (18) to (3), we obtain the duration D_{cB} for which the numbers of cells are equal. With $c\ T_S = 2\ L_S$, where T_S is the resonance period corresponding to the scatterer length, we have

$$D_{cB} = \frac{\pi}{\Theta \ln B} \frac{\ln g}{g - \sqrt{g}} T_S = \frac{313}{\Theta} \frac{\ln g}{g - \sqrt{g}} T_S. \tag{20}$$

The ratio D_{cB}/T_S only depends on the geometric progression g. With PML-A ($\Theta = 3$) and $g = 1.97$, it equals 125. Thus, using $g = 1.97$ with a 100-cell scatterer, the PML-B is thinner than the PML-A when the duration of the computation is longer than 125 resonance periods. We note that D_{cB}/T_S vary smoothly with g. From $g = 4$ to 1.5, it varies from 72 to 154 with $\Theta = 3$.

The implementation of the PML-B version in the FDTD method requires taking into account the transverse conductivities in the PML, and the equations of vacuum must be replaced by the MM equations in the inner domain. In principle, starting from the basic PML, such modifications are small, as we experienced with [8]. When implementing a Huyghens surface in the MM, one must take care that the magnitude of the incident wave must decrease according to (13). Using the PML-B version, the computational time per cell is increased in both the PML-B and the inner domain. In 3-D, there are 62 operations in the PML-B cells instead of 56, and 42 in the MM cells instead of 36 in vacuum. By supposing that the computational time is proportional to the number of operations, the expected increase is in the range 12%–17%. For domains whose sizes are about 100 cells, this extra time is equivalent to the addition of two or three cells to the thickness of the basic PML. Actually, numerical experiments have shown that the cost of PML-B may be far smaller. For cubic 100-cell domains, on a workstation the extra costs were equivalent to the addition of less than 1/10 cell to the PML thickness. This is due to the fact that the extra operations are multiplications of the components by factors which are constant in the loops on mesh index, resulting in a very fast treatment by the computer. With such a negligible extra time, PML-B is more efficient than PML-A when the solution of the problem to be solved is required for more than the time D_{cB} given by (20) with $\Theta = 3$.

V. Operator on the Outer Boundary

With the intention of reducing the PML thickness, a natural idea is the replacement of the perfect conductor condition set on the outer boundary by one of the previous methods of free-space simulation [5], [6]. We may expect that $R(0)$ could be increased so that N from (3) could be decreased. We have experimented with the following operators, in which E_0 and E_1 are an electric component, on the boundary and one cell from the boundary, respectively:

$$E_0^{n+1} = e^{-\frac{\sigma_{1/2}\Delta x}{\varepsilon_0 c}} E_1^n \tag{21}$$

$$E_0^{n+1} = e^{-\frac{\sigma_{1/2}\Delta t}{\varepsilon_0}} [(1-\alpha)E_0^n + \alpha E_1^n] \quad \alpha = \frac{c\Delta t}{\Delta x} \tag{22}$$

$$E_0^{n+1} = e^{-\frac{\sigma_{1/2}\Delta x}{\varepsilon_0 c}} [(2-\beta)E_1^n + (\beta - 1)E_1^{n-1}]$$

$$\beta = \frac{\Delta x}{c\Delta t}. \tag{23}$$

In a vacuum ($\sigma_{1/2} = 0$), the first operator (21) is the space–time extrapolation in [6]. The field on the boundary is set equal to the field that was one cell from the boundary at the previous time step. It is a first-order operator with zero reflection at incidence $\cos\theta = c\Delta t/\Delta x$. We introduced the exponential coefficient to take into account the absorption in the PML. The second operator has been obtained by considering that the unknown field was $c\ \Delta t$ from the boundary at the previous time step, and the last that the unknown field was one cell from the boundary $\Delta x/c$ before. Both are first-order operators with zero reflection at normal incidence.

Fig. 6 shows some results computed using PML's having normal reflections in the range 1%–30%, either with or without (21). With (23) the results were about the same, and with (22) they were worse. It is clear that the results are improved by using (21) in place of perfect electric conditions. But this does not allow $R(0)$ to be widely increased, so that the thickness (3) cannot be significantly decreased. Nevertheless, even a small decrease of N may result in a small saving of computational time, since the expected cost of (21) is very small due to its

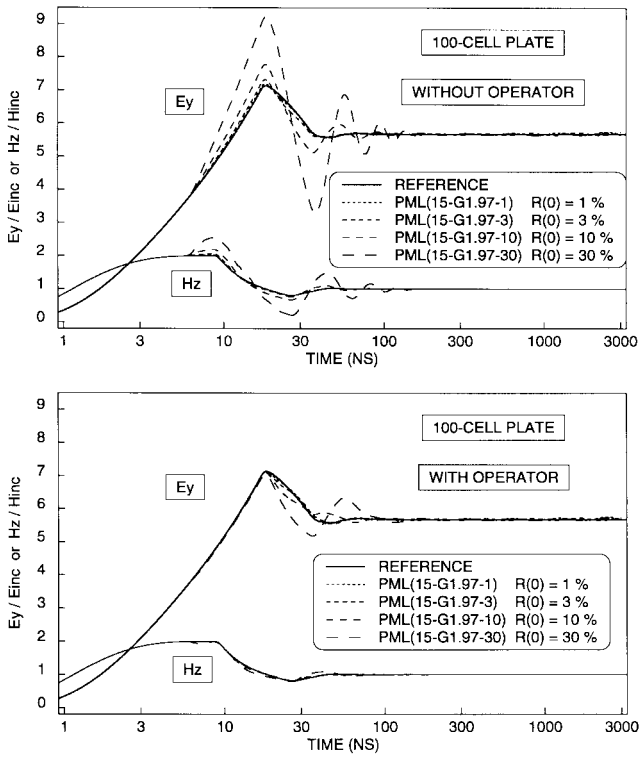

Fig. 6. Electric and magnetic fields on 20-cell and 100-cell plates computed with an operator on the outer boundary and various reflections $R(0)$.

simplicity. Actually, we have performed no 3-D tests until now.

VI. Expanded Mesh in the PML

With absorbing boundary conditions such as [5] and [6], a usual method to reduce the overall number of FDTD cells in the computational domain has been the use of cells growing geometrically from the scatterer to the boundary conditions. With the PML method, such an expanded mesh may be used within the PML to reduce its number of cells. This can be understood by considering the normal reflection of a PML, in which δ is the PML thickness and ρ the distance from the interface

$$R(0) = \exp\left[-\frac{2}{\varepsilon_0 c}\int_0^{\delta}\sigma(\rho)d\rho\right]. \tag{24}$$

By expanding the step size $\Delta\rho$ of the grid, the physical thickness δ is increased so that the required reflection $R(0)$ can be achieved with a reduced number of cells in the PML thickness.

To minimize the numerical reflection, the conductivities $\sigma_n(L)$ must grow geometrically in the expanded mesh. The mesh and profile of conductivity presented below allow this condition to be satisfied. Denoting by h the expansion factor of the grid and Δx the step size in the inner domain, the locations of the computational points are chosen so that

$$\rho(L) = \sqrt{h}\frac{h^L - 1}{h-1}\Delta x \qquad (L = 0, 1/2, 1, 3/2, 2, ...) \tag{25}$$

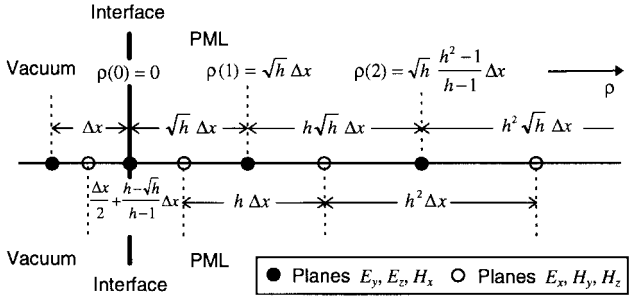

Fig. 7. The expanded mesh growing geometrically.

resulting in the following steps $\Delta\rho$

$$\Delta\rho(0) = \left(\frac{1}{2} + \frac{h-\sqrt{h}}{h-1}\right)\Delta x \tag{26a}$$

$$\Delta\rho(L>0) = h^L \Delta x. \tag{26b}$$

This mesh is summarized in Fig. 7. The half-cell (distance between adjacent computational points) grows geometrically with ratio $\sqrt{h}$, while the cell grows with ratio h. As found in the past, such a feature slightly reduces the intergrid reflection in expanded meshes. The profile of conductivity $\sigma(\rho)$ is chosen as

$$\sigma(\rho) = \sigma_0 g^{\ln\left[1+(h-1)\rho/\sqrt{h}\Delta x\right]/\ln h}. \tag{27}$$

Replacing ρ by (25) in (27), we note that the analytical conductivity at mesh points is $\sigma_0 g^L$, as in a constant mesh with profile (2). From (24), (25), and (27), the reflection $R(0)$ is

$$R(0) = \exp\left[-\frac{2\sigma_0}{\varepsilon_0 c}\int_0^{\sqrt{h}\frac{h^N-1}{h-1}\Delta x} g^{\ln\left[1+(h-1)\rho/\sqrt{h}\Delta x\right]/\ln h} d\rho\right]. \tag{28}$$

With $u = \Delta x \ln\left[1+(h-1)\rho/\sqrt{h}\Delta x\right]/\ln h$ we obtain

$$R(0) = \exp\left[-\frac{2\sigma_0}{\varepsilon_0 c}\frac{\sqrt{h}\ln h}{h-1}\int_0^{N\Delta x}(gh)^{\frac{u}{\Delta x}}du\right] \tag{29}$$

from which

$$R(0) = \exp\left[\frac{2}{\varepsilon_0 c}\frac{\sqrt{h}\ln h}{h-1}\frac{1-(gh)^N}{\ln gh}\sigma_0\Delta x\right]. \tag{30}$$

Calculating the numerical conductivity $\sigma_n(L)$ as the average value in the cell $\Delta\rho(L)$ around location L also involves an integral like that in (28). Substituting σ_0 from (30) in the result of this calculation, the following $\sigma_n(L)$ are obtained:

$$\sigma_n(0) = \frac{\varepsilon_0 c}{2\Delta x}\frac{2h-2}{3h-2\sqrt{h}-1}\frac{1-\sqrt{gh}}{(gh)^N-1}\ln R(0) \tag{31}$$

$$\sigma_n(L>0) = \frac{\varepsilon_0 c}{2\Delta x}\frac{(1-gh)\ln R(0)}{\sqrt{gh}[(gh)^N-1]}g^L. \tag{32}$$

First, we note that the numerical conductivity grows geometrically with ratio g as in a constant grid, so that the numerical

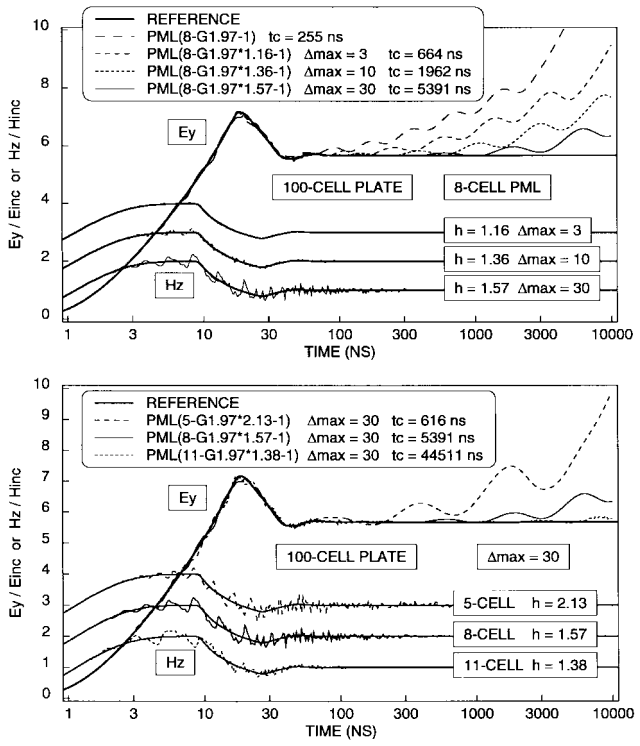

Fig. 8. Electric and magnetic fields on a 100-cell plate computed with various expanded meshes. In each part, two out of three magnetic fields are arbitrarily shifted upward to make more visible the numerical noise.

reflection is optimized. Second, (31) and (32) are nothing but [4, Eq. (12), (13)], with an additional term in (31) and g replaced by gh in both formulas. From (1) and (31) we deduce the number of cells N that is required for a computational duration D_c

$$N = \frac{1}{\ln gh} \ln \left[1 - \frac{c}{4\pi} \frac{2h-2}{3h-2\sqrt{h}-1} (\sqrt{gh}-1) \ln R(0) \frac{\Theta}{\Delta x} D_c \right]. \quad (33)$$

This formula is (3), with the additional term of (31) and g replaced by gh. For the usual values of h, the additional term is close to one (in the range 0.92–1 with $1 < h < 2$). As a consequence, the thickness N of the expanded mesh is about that of the constant mesh having a profile of conductivity of ratio gh.

Numerical experiments are shown in Fig. 8 with the 100-cell plate. The electric and magnetic fields are shown at the end and the center of the plate, respectively. The incident wave was a unit step of 1-ns rise time. The PML's in an expanded grid are denoted as PML(N-Gg*h-R(0)). In the figure, the parameter $\Delta_{\max}$ is the ratio of the largest cell $\Delta\rho(N\text{-}1/2)$ to the inner cell Δx. From (26b) we have

$$\Delta_{\max} = h^{N-1/2}. \quad (34)$$

The upper part of Fig. 8 shows some results computed using an 8-cell PML and three values of h. As h increases, the cutoff time t_c increases, and the electric field later departs from the reference solution. As expected, spurious reflection occurs from the expanded grid since the highest frequencies cannot propagate through the largest cells. This reflection is more visible on the magnetic field. It is mainly determined by the size of the largest cells, as illustrated in the lower part of Fig. 8. With the same ratio $\Delta_{\max} = 30$, three computations were performed with 5-, 8-, and 11-cell PML's, and then, quite different factors h. All the spurious reflections are about the same. Thus, using an expanded mesh, the critical parameter is the largest cell, i.e., the ratio $\Delta_{\max}$.

Fig. 8 suggests that only moderate $\Delta_{\max}$ could be used. Experiments with 3-D scatterers have shown spurious reflection like that in Fig. 8. Furthermore, with a given $\Delta_{\max}$ we have observed that the reflection slightly decreases as the number of cells in the scatterer length increases. In practice, from such various experiments with the 3-D scatterers that the computers can nowadays process (50–200 cell long), $\Delta_{\max}$ in the range 3–5 produces very small high-frequency spurious reflection.

The above values of $\Delta_{\max}$ could appear as small. Nevertheless, they allow a significant reduction of the PML thickness to be achieved due to the fact that most absorption is located within the outer cells of the PML. With 100-cell scatterers whose ratio g is about 2, at least one cell is saved with $\Delta_{\max} = 3$, and two cells with $\Delta_{\max} = 5$. In 3-D, such decreases result in reductions of the overall cost of the FDTD computation larger than 5% and 10%, respectively. Thus, since the cost of an expanded mesh is zero (no additional operation in the loop on time), using a moderate expanded mesh is a valuable means to reduce the computational cost of PML's.

VII. A 3-D Experiment

Fig. 9 illustrates the decrease of the PML thickness achieved by using the PML-A interface in conjunction with an expanded mesh. The scatterer is the 100*20-cell plate of zero thickness used in [2]. Two incident waves were considered—the unit step and the two-exponential pulse of width 100 ns also used in [2]. With a 7-cell basic PML the electric field departs from the reference before 40 ns. With either a PML-A or a $\Delta_{\max} = 5$ expanded grid, the field departs around 100 ns. With both improvements, the results are valid for the 300 ns in Fig. 9. Obtaining such results requires a 11-cell basic PML. The lower part of Fig. 9 shows that the spurious reflection from the expanded mesh is very small. For this test, from the 11-cell PML to the 7-cell PML, the computational time was reduced by a factor of two. For a cubic 100-cell scatterer the reduction would be at least equal to 20%.

VIII. Conclusion

As early as the initial experiments with the PML method, investigating the numerical reflection appeared as a challenge of prime importance to make this method efficient and reliable. We mainly focused on wave-structure interactions, a class of problems including important applications of the FDTD method as EMC and RCS calculations. The first step of investigations [4] was an heuristic analysis of the numerical reflection from which an optimum PML was designed to allow accurate near fields to be computed with computational requirements as small as possible. The second step consisted of searching for improvements to this optimum PML, with the

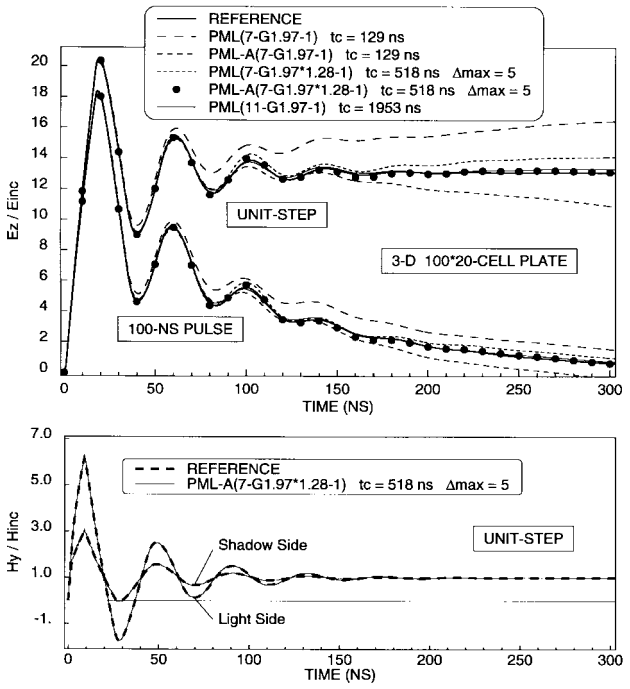

Fig. 9. Electric and magnetic fields on a 3-D 100^*20-cell plate computed with PML, PML-A, PML with an expanded mesh, and PML-A with an expanded mesh. Two incident waves are considered, a unit step (rise-time 1 ns), and a two-exponential pulse (rise-time 1 ns, descent-time 100 ns). The magnetic field is plotted at the center of the plate on both light and shadow sides.

intention of reducing its thickness. Four improvements have been discussed in the present paper.

The first two improvements, namely the PML-A and PML-B versions of the PML method, were thought up from the interpretation of the numerical reflection [4]. The last two are natural ideas: first, using a traditional absorbing condition on the outer boundary of the PML, and second, using an expanded FDTD grid. In practice, the PML-A version and the expanded grid are probably the most useful improvements. They can be used in most applications and they significantly decrease the PML thickness. Contrary to waveguide problems investigated in [10], using an operator on the outer boundary seems not very promising, at least from our tests. The PML-B version might be viewed as a theoretical bound to the PML thickness, but also it may be useful in some EMC applications requiring long-time calculations.

In conclusion, the improved versions of the optimum PML allow the numerical reflection to be controlled and made negligible with relatively thin PML's located close to scattering structures. As a consequence, the PML method is very efficient in terms of computational requirements. This efficiency might be increased in future—first, by using the optimum PML in conjunction with a formulation involving a reduced set of unknowns [11], [12], [13]; second, from a theory predicting the numerical reflection observed in wave-structure interaction problems. Starting from [14], such a theory has been recently investigated [15], providing us with a new understanding from which new improvements to the optimum PML might be hoped for.

REFERENCES

[1] J.-P. Bérenger, "A perfectly matched layer for the absorption of electromagnetic waves," *J. Comput. Phys.*, vol. 114, no. 2, pp. 185–200, Oct. 1994.
[2] ———, "Three-dimensional perfectly matched layer for the absorption of electromagnetic waves," *J. Comput. Phys.*, vol. 127, no. 2, pp. 363–379, Sept. 1996.
[3] K. S. Yee, "Numerical solution of initial boundary value problems involving Maxwell's equations in isotropic media," *IEEE Trans. Antennas Propagat.*, vol. 14, pp. 302–307, May 1966.
[4] J.-P. Bérenger, "Perfectly matched layer for the FDTD solution of wave-structure interaction problems," *IEEE Trans. Antennas Propagat.*, vol. 44, pp. 110–117, Jan. 1996.
[5] B. Engquist and A. Majda, "Absorbing boundary conditions for the numerical simulation of waves," *Math. Comput.*, vol. 31, no. 139, pp. 629–651, July 1977.
[6] R. Higdon, "Absorbing boundary conditions for difference approximations to the multi-dimensional wave equation," *Math. Comput.*, vol. 47, no. 176, pp. 437–459, Oct. 1986.
[7] J.-P. Bérenger, "A perfectly matched layer for free-space simulation in finite-difference computer codes," *Ann. Télécommunicat.*, vol. 51, no. 1/2, pp. 39–46, Jan. 1996.
[8] ———, The DIFRAC code, version 6-1993, unpublished.
[9] ———, "La méthode PML en Compatibilité Electromagnétique," in *Proc. CEM Symp.*, Lille, France, Sept. 1996, pp. 327–332.
[10] C. M. Rappaport, "Perfectly matched absorbing boundary conditions based on anisotropic lossy mapping of space," *IEEE Microwave Guided Wave Lett.*, vol. 5, pp. 90–92, Mar. 1995.
[11] R. Mittra and Ü. Pekel, "A new look at the perfectly matched layer (PML) concept for the reflectionless absorption of electromagnetic waves," *IEEE Microwave Guided Wave Lett.*, vol. 5, pp. 84–86, Mar. 1995.
[12] Z. S. Sacks, D. M. Kingsland, R. Lee, and J.-F. Lee, "A perfectly matched anisotropic absorber for use as an absorbing boundary condition," *IEEE Trans. Antennas Propagat.*, vol. 43, pp. 1460–1463, Dec. 1995.
[13] S. D. Gedney, "An anisotropic perfectly matched layer absorbing media for the truncation of FDTD lattices," Tech. Rep. EMG-95-006, Univ. Kentucky, May 1995.
[14] J. De Moerloose and M. A. Stuchly, "Behavior of Bérenger's ABC for evanescent waves," *IEEE Microwave Guided Wave Lett.*, vol. 5, pp. 344–346, Oct. 1995.
[15] J.-P. Bérenger, "Optimized PML for wave-structure interaction problems," presented at *PIERS'96 Symp.*, Innsbruk, Austria, July 1996.

Jean-Pierre Bérenger, for photograph and biography, see p. 117 of the January 1996 issue of this TRANSACTIONS.